Detection of a parsec-scale jet in a radio-quiet narrow-line Seyfert 1 galaxy with highly accreting supermassive black hole

Downloaded from: https://research.chalmers.se, 2026-10-15 05:14 UTC

Citation for the original published paper (version of record):
Yao, S., Yang, X., Gu, M. et al (2021). Detection of a parsec-scale jet in a radio-quiet narrow-line Seyfert 1 galaxy with highly
accreting supermassive black hole. Monthly Notices of the Royal Astronomical Society, 508(1): 1305-1313. http://dx.doi.org/10.1093/mnras/stab2651

N.B. When citing this work, cite the original published paper.

research.chalmers.se offers the possibility of retrieving research publications produced at Chalmers University of Technology. It covers all kind of research output: articles, dissertations, conference papers, reports etc. since 2004. research.chalmers.se is administrated and maintained by Chalmers Library

(article starts on next page)

Monthly Notices of the ROYAL ASTRONOMICAL SOCIETY

MNRAS **508,** 1305–1313 (2021) https://doi.org/10.1093/mnras/stab2651
Advance Access publication 2021 September 16

Detection of a parsec-scale jet in a radio-quiet narrow-line Seyfert 1 galaxy with highly accreting supermassive black hole

Su Yao [1]★ Xiaolong Yang,[2,3]★ Minfeng Gu,[4] Tao An [2] Jun Yang [5] Luis C. Ho,[3,6] Xiang Liu,[7] Ran Wang,[3] Xue-Bing Wu[3,6] and Weimin Yuan[8]

[1]*Max-Planck-Institut für Radioastronomie, Auf dem Hügel 69, D-53121 Bonn, Germany*
[2]*Key Laboratory of Radio Astronomy, Shanghai Astronomical Observatory, Chinese Academy of Sciences, Shanghai 200030, China*
[3]*Kavli Institute for Astronomy and Astrophysics, Peking University, Beijing 100871, China*
[4]*Key Laboratory for Research in Galaxies and Cosmology, Shanghai Astronomical Observatory, Chinese Academy of Sciences, Shanghai 200030, China*
[5]*Department of Space, Earth and Environment, Chalmers University of Technology, Onsala Space Observatory, SE-439 92 Onsala, Sweden*
[6]*Department of Astronomy, School of Physics, Peking University, Beijing 100871, China*
[7]*Key Laboratory of Radio Astronomy, Xinjiang Astronomical Observatory, Chinese Academy of Sciences, 150 Science 1-Street, Urumqi 830011, China*
[8]*Key Laboratory of Space Astronomy and Technology, National Astronomical Observatories, Chinese Academy of Sciences, Beijing 100101, China*

Accepted 2021 September 10. Received 2021 September 10; in original form 2021 May 12

ABSTRACT

The jet in active galactic nuclei (AGN) is a key ingredient in understanding the co-evolution of galaxies and their central supermassive black holes (SMBHs). Unfortunately, the mechanism of jet launching and collimation is still elusive. The observational evidence of decreasing radio loudness with increasing Eddington ratio implies that the jet should be coupled with the accretion process. To further explore the relationship between the jet and accretion, it is necessary to extend our knowledge of the jet to an extreme end of the Eddington ratio distribution of AGN. Using Very Long Baseline Array (VLBA), we report the detection of the parsec-scale radio structure in Mrk 335, a radio-quiet narrow-line Seyfert 1 galaxy with an Eddington ratio close to/above unity. The VLBA image at 1.5 GHz reveals an elongated structure extending ∼20 pc in north–south direction with a peak flux density of 1.98 ± 0.05 mJy beam^{-1} and radio brightness temperatures as high as 6×10^7 K. This feature provides a strong evidence of a parsec-scale (bipolar) jet launched from a highly accreting SMBH. We discuss the result by comparing Mrk 335 with other highly accreting systems, e.g. Galactic black holes and tidal disruption events, and recall the discovery of collimated corona in the vicinity of SMBH in Mrk 335 by previous X-ray observations, whose relation to the parsec-scale radio jet should be explored by future simultaneous X-ray spectroscopy and high resolution radio observations.

Key words: galaxies: active – galaxies: individual: Mrk 335 – galaxies: jets – galaxies: nuclei – galaxies: Seyfert.

1 INTRODUCTION

The collimated outflowing plasma, also termed as 'jet', launched from active galactic nuclei (AGN) is suggested to be one of the important forms of AGN feedback that regulates the coevolution of supermassive black hole (SMBH) and their host galaxy (Fabian 2012; Kormendy & Ho 2013). The AGN jets typically peak their radiation in the radio band by synchrotron processes and could be luminous radio sources. However, only 15–20 per cent of the AGN are radio-loud (Urry & Padovani 1995; Ivezić et al. 2002), indicating that not all of the AGN launch jets. This raises the questions of why we only observe jets in a small fraction of AGN and how the jets are formed.

The observational evidence of a strong anticorrelation between the radio loudness parameter $\mathcal{R}$[1] and the bolometric luminosity expressed in Eddington units, i.e. Eddington ratios $\lambda_{\rm Edd}$, implies coupling of the jet and accretion process (Ho 2002, 2008; Greene, Ho & Ulvestad 2006; Sikora, Stawarz & Lasota 2007; Yang et al. 2020); the launch of jet may be dependent on the Eddington ratio and underlying physics such as the mass accretion rate, the state of accretion disc, and the growth of SMBH. But the detailed mechanism remains elusive. Given the anticorrelation of the radio loudness and the Eddington ratio, questions arise as to whether the collimation of outflows is suppressed as the Eddington ratio increases, and whether there is a limiting Eddington ratio above which the collimation is quenched. On the other hand, while the origin of radio core emission is clear in the radio-loud AGN as dominated by the non-thermal radiation from jets, the case of the radio-quiet AGN is more complex. With milli-arcsecond (mas) resolution radio images achieved by very long baseline interferometry (VLBI), it was found that some of the radio-quiet AGN reveal compact parsec-scale

★ E-mail: syao@mpifr-bonn.mpg.de (SY); yangxl@shao.ac.cn (XY)

[1]The radio loudness parameter $\mathcal{R}$ is defined as the ratio of radio-to-optical flux density, conventionally at 5 GHz and *B* band (4400Å), respectively, with $\mathcal{R} \approx 10$ as the dividing of radio-quiet and radio-loud AGN (e.g. Kellermann et al. 1989).

© The Author(s) 2021.
Published by Oxford University Press on behalf of Royal Astronomical Society. This is an Open Access article distributed under the terms of the Creative Commons Attribution License (http://creativecommons.org/licenses/by/4.0/), which permits unrestricted reuse, distribution, and reproduction in any medium, provided the original work is properly cited.

nuclear radio emission with brightness temperatures of $T_B \gtrsim 10^7$ K and occasionally accompanied by collimated features that provide the evidence of small, weak jets (e.g. Mundell et al. 2003; Middelberg et al. 2004; Giroletti & Panessa 2009; Doi et al. 2013; Panessa & Giroletti 2013; Wang et al. 2021), while others only show radio emission from the presumably star-forming region, disc wind, or hot corona (e.g. Gallimore, Baum & O'Dea 2004; Bontempi et al. 2012, see also Panessa et al. 2019 for a review). Questions arise as to why the collimated outflows do form in some radio-quiet AGN but not in others, and whether they are intrinsically different from their powerful analogues in blazars and radio galaxies.

Keeping in mind the above questions, we have proposed imaging observations on the central parsec-scale nuclear region of a sample of nearby radio-quiet narrow-line Seyfert 1 (NLS1) galaxies with accretion rates approaching to or exceeding the Eddington limit (Yang et al. 2020) using the Very Long Baseline Array (VLBA) of the National Radio Astronomy Observatory (NRAO). The NLS1 galaxies are believed to rapidly growing their central SMBHs that are in a relatively low-mass range of $\sim 10^6$–10^8 $M_\odot$ (Zhou et al. 2006). They are often being radio-quiet and have a lower radio-loud fraction compared to the normal Seyfert galaxies and quasars (Yuan et al. 2008). While the parsec-scale jets have been detected in the radio-loud NLS1 galaxies (e.g. Doi, Asada & Nagai 2011; Gu et al. 2015), the case is still elusive for the radio-quiet ones, especially when it approaches the highest Eddington ratio regime. In recent years, the work dedicated to study parsec-scale region of the radio-quiet NLS1 galaxies has found jet features in several of them (Doi et al. 2013), but only Mrk 1239 has a reliably measured Eddington ratio close to/higher than one[2] (Doi et al. 2015; Pan et al. 2021). So, further studies on the parsec-scale nuclear region in radio-quiet NLS1 galaxies with highest Eddington ratios should provide general clues of the interplay between the jet and accretion disc. Our observations will not only search the signature of jet in these radio-quiet highly accreting systems, but also extend our knowledge of the parsec-scale radio properties of AGN to a rarely explored parameter space.

In this paper, we present the result of our VLBA observation on Mrk 335 ($z = 0.025785$; Huchra, Vogeley & Geller 1999) as one of the outcomes in the course of our ongoing project (Yang et al. in preparation). Mrk 335 is a well-known NLS1 galaxy with an SMBH weighing $\sim 10^7$ $M_\odot$ (Peterson et al. 2004; Grier et al. 2012; Du et al. 2014) hosted in a disc galaxy (Kim et al. 2017). It has been extensively observed in optical (e.g. Peterson et al. 2004; Grier et al. 2012; Du et al. 2014) and X-rays (e.g. Grupe et al. 2008; Gallo et al. 2018, 2019; Komossa et al. 2020; Tripathi et al. 2020). Based on its optical luminosity and hard X-ray spectrum, Mrk 335 was suggested to host a candidate of super-Eddington accreting massive black hole (Wang et al. 2013, 2014). But the knowledge of its radio emission is rather limited. Mrk 335 has been observed by the VLA with various angular resolution (see Table 1 and the literatures therein). All these observations reveal a compact unresolved weak source. Based on the nuclear optical flux derived from the decomposition of *HST* *V*-band (F550M) image (Du et al. 2014) and an assumed optical spectral index of $\alpha = -0.5$ ($S_\nu \propto \nu^\alpha$), the radio loudness of Mrk 335 is estimated to be $\mathcal{R} \approx 0.8$, falling into the radio-quiet category. Interestingly, a collimated outflow near the accretion disc has been discovered in Mrk 335 from the X-ray spectral analysis by Gallo et al. (2019). Here, we report the detection of a parsec-scale jet feature in Mrk 335 using VLBA. Throughout this work, a cosmology is assumed with $H_0 = 70\,\mathrm{km\,s^{-1}\,Mpc^{-1}}$, $\Omega_\Lambda = 0.73$, and $\Omega_M = 0.27$; 1 mas corresponds to a scale of 0.512 pc at the distance of Mrk 335.

[2]Another one is Ark 564, the VLBI image of which shows an elongated structure as reported by Lal, Shastri & Gabuzda (2004). However, it is noted in their paper that the (u, v) coverage obtained was relatively poor, and they do not feel confident that the elongated feature is an accurate representation of the VLBI-scale structure of the source.

Table 1. Previous VLA observations on Mrk 335.

Frequency (GHz) (1)	Flux density (mJy) (2)	Date (3)	Resolution (4)	Reference (5)
1.4	4.1 ± 0.9	1983.07	1.″5	E87
	6.19 ± 0.29	1992.12	2″	N99,Y20
	7.3 ± 0.4	1993.11	45″	C98
5	3.9	1982.11-1983.05	18″	K89,M93
	3.3 ± 0.2	1983.07	15″	E87
	3.58 ± 0.05	2003.06[a]	0.″3	L06
	3.21 ± 0.02	2015.07	0.″4	B18,Y20
8.4	2.05	1991.06	0.″3	K95
	2.23	1992.04	2.″5	K95
	2.14 ± 0.06	1992.12	0.″3	N99,Y20
	2.3[b]	1997.01-1999.04	1–3″	B05

Notes. E87: Edelson (1987); N99: Nagar et al. (1999); C98: Condon et al. (1998); K89: Kellermann et al. (1989); M93: Miller, Rawlings & Saunders (1993); L06: Leipski et al. (2006); B18: Berton et al. (2018); Y20: Yang et al. (2020); K95: Kukula et al. (1995); B05: Barvainis et al. (2005).
[a]This observation date is obtained from the VLA data archive.
[b]This measurement is the mean flux density obtained from a number of observations (see B05).

2 OBSERVATIONS AND DATA REDUCTION

2.1 VLBA observation and data reduction

We observed Mrk 335 on 2018 September 15 using 10 antennas of the VLBA (project code: BY145, P.I. Yao). The observation was made in the *L* band with a central frequency of 1.548 GHz ($\lambda \sim 19.4$ cm) and a total bandwidth of 256 MHz. The observation was performed in the phase-referencing mode: the target field was observed for 1.53 h in 4-min scans, interleaved with 1-min scans of the phase referencing calibrator J0004 + 2019 (RA: $00^h04^m35.^s758287$, Dec: $+20^\circ19'42.''31786$, J2000), with the phase calibrator located at 0.42 deg away from the target. We also inserted a scan of the bright radio source 3C 454.3 for fringe and bandpass calibration. The data were recorded at 2 Gbps in dual circular polarization. The raw data was correlated with the software correlator DiFX (Deller et al. 2007, 2011).

The visibility data were calibrated using the NRAO Astronomical Image Processing System (AIPS; Greisen 2003) following the standard procedure. A prior amplitude calibration was performed with the system temperatures and the antenna gain curves. The Earth's orientation parameters were obtained and corrected by using the measurement from the U.S. Naval Observatory data base and the ionospheric dispersive delays were corrected according to a map of total electron content provided by the GPS satellite observations. The opacity and parallactic angle corrections were also applied according to the attached information in data. Phase delay from the instrument was removed by fringe-fitting over the scan of 3C 454.3. The bandpass solutions were also determined from the fringe finder calibrator 3C 454.3. Finally, we performed a global fringe-fitting on the phase-referencing calibrator J0004 + 2019. The calibrated data of the phase-referencing source J0004 + 2019 was averaged in AIPS and then exported into DIFMAP software package (Shepherd 1997) for imaging and self-calibration. J0004 + 2019 shows a bright

and compact structure in our observation, consistent with the model assumed in fringe-fitting in AIPS.

The deconvolution of the visibility data was performed in DIFMAP. The source is relatively weak, with a peak flux density of only 1.98 ± 0.05 mJy peak^{-1} and a signal-to-noise ratio of ∼47. Therefore, we did not perform the self-calibration procedure.

We also check the historical VLBA observations of Mrk 335 in projects BB0056 and BG0093 from the NRAO archive. The observation in project BB0056 is performed in the *X*-band on 1996 June 9 with a total bandwidth of 32 MHz and a total on-source time of 48 min, while the observation in project BG0093 is performed in the *S*/*X*-band[3] on 1999 July 9 with a total bandwidth of 192 MHz and also a total on-source time of 48 min. We have processed all these data following similar procedures as described above. Unfortunately, Mrk 335 is not detected in the *X*-band observation during BB0056 and BG0093. This is consistent with the result reported by Blundell & Beasley (1998), which also analyzed BB0056 data and gave an upper limit of the flux density <0.8 mJy at 8.4 GHz. In the *S*-band (2.3 GHz), Mrk 335 is only marginally detected with a very low signal-to-noise ratio of 6.17 and a peak flux density of 0.82 ± 0.24 mJy beam^{-1}.

2.2 Archival VLA data

To compare the radio morphology of Mrk 335 on different scales, we also retrieve two sets of archival data observed on 1992 December 31 using the VLA A-array configuration in the *L* band and *X* (AM0384). The *L*-band data were taken at a central frequency of 1.4 GHz, and the *X*-band data were taken at a central frequency of 8.4 GHz. Both observations have a total bandwidth of 100 MHz. The data are manually calibrated using the Common Astronomy Software Application (CASA v5.1.1; McMullin et al. 2007) following the standard procedures described in CASA Cookbook. The final images are made using the DIFMAP software package. The detailed description of the data reduction and analysis can be found in Yang et al. (2020).

3 RESULTS

3.1 Source structures

The naturally weighted images of Mrk 335 observed by the VLA A-array configurature at 1.4 and 8.4 GHz, and by the VLBA at 1.5 GHz are shown in Figs 1(a), (b), and (c), respectively. As can be seen, while Mrk 335 is compact, unresolved in the VLA images, it reveals an elongated structure extending along the south–north direction in the VLBA image. The structure is resolved at ∼40 mas, corresponding to a projected physical scale of ∼20 pc at the redshift of Mrk 335. We also show the naturally weighted image of the archival *S*-band (2.3 GHz) data in Fig. 2. Due to the short exposure time and narrow bandwidth, the 2.3 GHz image has a low signal-to-noise ratio and only recovers the brightest component (southern structure) as seen in the 1.5 GHz image. Thus, we only consider the structure revealed by the new VLBA data at 1.5 GHz in the following analysis.

In order to further explore the structure seen in 1.5 GHz VLBA image, we perform a two-dimensional Gaussian model fitting to the visibility data using the `modelfit` procedure in the DIFMAP package. The best-fitting five components are listed in Table 2. The uncertainty of the flux density of each component is estimated by combining the fitting error with the initial calibrating error (Hovatta et al. 2012). The entire structure of Mrk 335 has a total flux density of 6.46 ± 0.06 mJy. The positions and sizes of the best-fitting five components are displayed in Fig. 1 as the red circles, which likely reveals an S-shaped distribution.

The *Gaia* mission (Gaia Collaboration 2016) has reported an optical position of Mrk 335 as RA = $00^{h}06^{m}19^{s}.537304 \pm 0^{s}.00001$, Dec = $+20^{\circ}12'10''.61670 \pm 0''.0002$ (the black cross in Fig. 1c). As can be seen in the figure, even considering the positional uncertainties of *Gaia* and the radio components, there is still a significant offset between the optical position and the centre of nearest radio component. With *Gaia* position as reference, the north and south radio components are, respectively, labelled as N2, N1 and S1, S2, S3. The symmetric distribution indicates a bipolar structure, with 'S' (bright) components being the approaching jet boosting radio emission and 'N' (faint) components being the receding jet fading away.

3.2 Radio brightness temperature

We calculate the radio brightness temperature for each model component from

$$T_{\rm B} = 1.8 \times 10^{9}(1+z)\frac{S_{\nu}}{\nu^{2}\phi^{2}} \quad (1)$$

in Kelvin (K, Ulvestad, Antonucci & Barvainis 2005) in the rest frame of Mrk 335, where z is the redshift, S_{ν} is the integrated flux density in mJy at the observing frequency ν in GHz, and ϕ is the fitted full width at half-maximum of the Gaussian components in units of mas. All the Gaussian components have the radio brightness temperature $T_{\rm B} > 10^{6}$ K and the component 'S2' has the highest brightness temperature of $T_{\rm B} \approx 6.2 \times 10^{7}$ K (Table 2).

4 DISCUSSION

At parsec scales, we have resolved Mrk 335 at 1.5 GHz into an elongated structure. The two-dimensional Gaussian model fitting to the visibility data has revealed five components distributed along the elongated structure, among which 'S1' and 'S2' components have $T_{\rm B} > 10^{7}$ K, indicating the non-thermal emission from jet. This provides a strong evidence for a parsec-scale jet launched by the SMBH in Mrk 335. As mentioned in Section 1, although the detailed physical mechanism for launching a jet is still elusive, it is generally suggested that the jet is coupled with the accretion process. Any detection of jet features in an object with accretion rate close to or above the Eddington limit would be of high value for the investigation of jet-accretion disc coupling. In the following, we discuss the Eddington ratio of Mrk 335, the origin of its radio emission, and the implication for its jet formation based on our detection.

4.1 Eddington ratio of Mrk 335

Based on the reverberation mapping technique, the estimations of the black hole mass of Mrk 335 ranges from 8.3 × 10^{6} to 2.6 × 10^{7} $M_{\odot}$ (Peterson et al. 2004; Grier et al. 2012; Du et al. 2014), much lower than those in the classical blazars and radio galaxies (e.g. Falomo, Kotilainen & Treves 2002; Barth, Ho & Sargent 2003). Besides the black hole mass, the determination of Eddington ratio requires an estimate of the bolometric luminosity $L_{\rm bol}$ that is the integration of thermal emission released by the accretion process. A direct way

[3]We note that the observing band of BG0093 in the NRAO archive is wrongly marked as *L*-band.

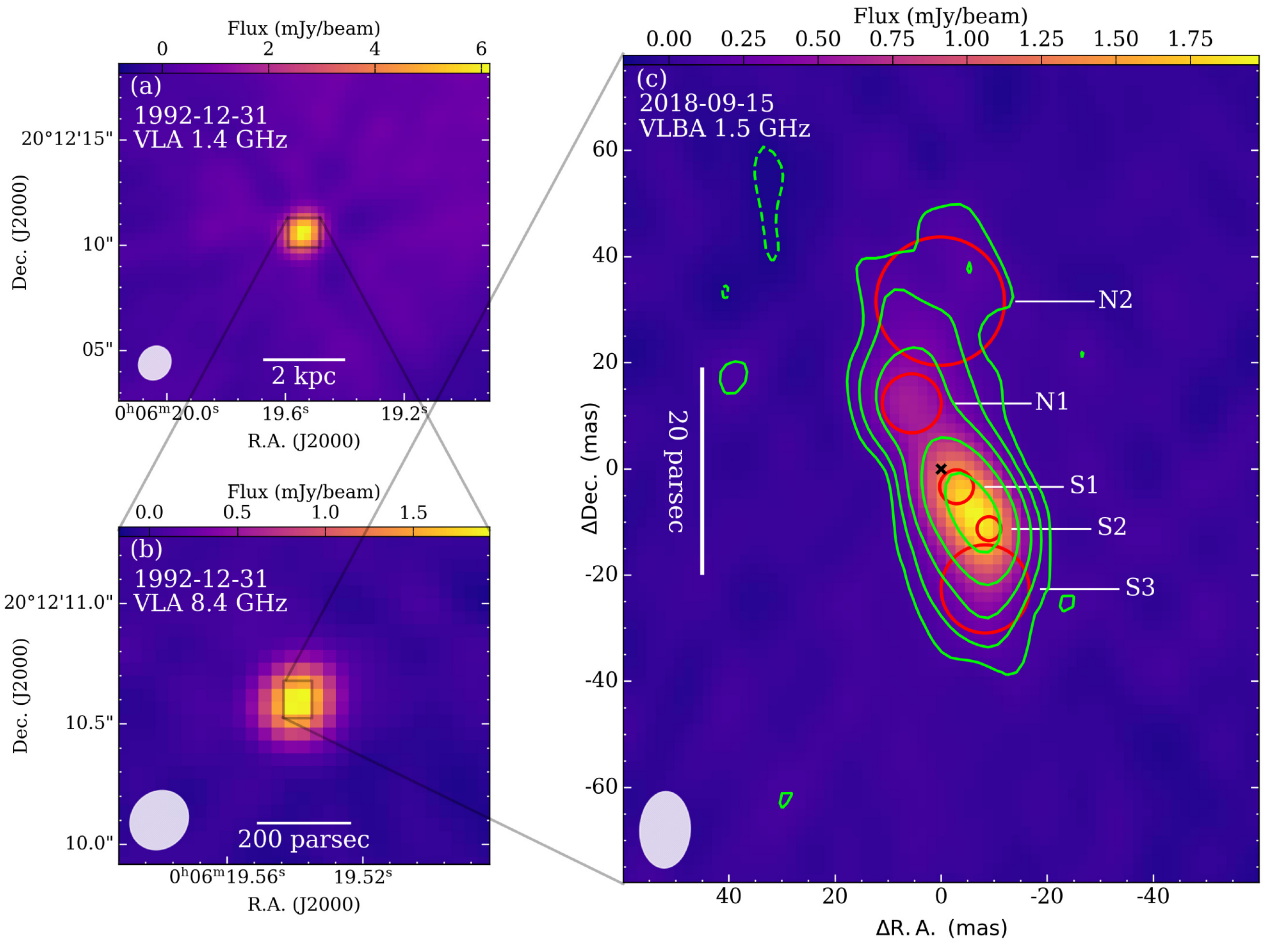

Figure 1. (a) The VLA 1.4 GHz image of Mrk 335. (b) The VLA 8.4 GHz image of Mrk 335. (c) The VLBA 1.5 GHz image of Mrk 335. The green contours in the VLBA image are plotted as $3\sigma \times (-1, 1, 2, 4, 8, 16)$, where $\sigma = 0.03$ mJy beam^{-1} is the rms noise. The peak flux density is 1.98 ± 0.05 mJy beam^{-1}. The elongated jet structure is fitted using the two-dimensional Gaussian models. The red circles mark the locations and sizes of the best-fitting Gaussian components. The optical position of Mrk 335 obtained by *Gaia* is represented by the black cross. The synthesized beam size is illustrated as an ellipse at the lower left corner of each image.

to estimate $L_{\rm bol}$ is to integrate the luminosity over a set of broad-bands dominated by the emission from accretion disc. Elvis et al. (1994) have constructed a spectral energy distribution (SED) from radio to X-rays of Mrk 335 and calculated the integral luminosity as $\sim 3 \times 10^{45}$ erg s^{-1} by simply interpolating through the observed data, which would yield an Eddington ratio of $\lambda_{\rm Edd} \approx 0.9$–3 considering the black hole mass range from the reverberation mapping. Vasudevan & Fabian (2009) have built two sets of simultaneous SEDs from optical to X-rays of Mrk 335, one of which was in its historical low X-ray flux state (Grupe et al. 2008). They calculated the integral bolometric luminosities based on the accretion disc (optical/UV) and the power-law (X-ray) model fitted to the data. The bolometric luminosities are 2×10^{45} and 1×10^{45} erg s^{-1}, respectively, at those two epochs, which would yield an Eddington ratio of $\lambda_{\rm Edd} \approx 0.3$–1.9.

There are several main factors contributing to the uncertainty of $L_{\rm bol}$. One is the lack of extreme ultraviolet (EUV) data, where the emission from Mrk 335's accretion disc is supposed to peak. While the simple interpolation of the EUV gap between optical and X-rays may lead to an underestimation of $L_{\rm bol}$, the physically reasonable estimate of EUV peak is model-dependent. Another one that could lead to the underestimation of $L_{\rm bol}$ is the internal extinction of the optical/ultraviolet emission. On the other hand, the contamination from the host galaxy can lead to an overestimation, mainly at longer wavelength, of $L_{\rm bol}$. In optical, the host galaxy contribution to the emission at 5100 Å was estimated as $\lesssim 20$ per cent from a decomposition of Mrk 335 *HST* image (Bentz et al. 2009; Du et al. 2014). Finally, the variability can also lead to the uncertainties in $L_{\rm bol}$. The flux of Mrk 335 varied by only a few per cent in the optical and by ~ 20 per cent in the UV (Du et al. 2014; Gallo et al. 2018). Meanwhile, it has exhibited much higher variability in X-rays by a factor of $\sim$50 (e.g. Gallo et al. 2018; Tripathi et al. 2020). However, since the coronal optical emission lines, which are supposed to be driven by EUV and soft X-rays, do not vary much in Mrk 335 (Grupe et al. 2008), it was suggested that such huge X-ray variability is due to the variable column density and covering factor of the X-ray absorbers near the SMBH (Komossa et al. 2020). Therefore, even considering the above uncertainties of $L_{\rm bol}$, the Eddington ratio of Mrk 335 is still high.

At last, we should note that, according to the current understanding of the accretion physics, the 'slim disc' is used to describe the accretion process around SMBH when Eddington ratio approaches unity (Abramowicz et al. 1988; Mineshige et al. 2000). The optical depth of such slim disc is so large that the majority of photons will be trapped in the disc until advected into the black hole rather than

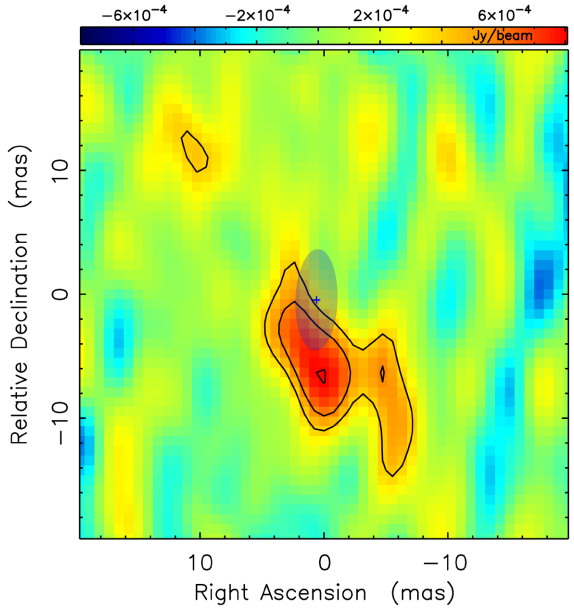

Figure 2. The archival VLBA S-band (2.3 GHz) image of Mrk 335 (project ID: BG0093). The image was produced by using a natural weight. The contours are plotted as $3\sigma \times (-1,\ 1,\ 1.41,\ 2,\ 2.82)$, where $\sigma = 0.13$ mJy beam^{-1} is the rms noise. The blue cross marks the location of the *Gaia* detection of Mrk 335. The beam is centred on *Gaia* position to show a VLBI positional uncertainty, with its size of 8.31 × 3.47 mas and a position angle of −2.81°.

Table 2. Model-fitting results of 1.5 GHz image obtained by our VLBA observation on Mrk 335.

Comp.	Flux density (mJy)	Size (mas)	$\Delta\alpha$ (mas)	$\Delta\delta$ (mas)	σ_Δ (mas)	T_B (K)
(1)	(2)	(3)	(4)	(5)	(6)	(7)
N2	0.97 ± 0.01	24.18	0.14	31.55	0.38	1.3×10^6
N1	1.06 ± 0.01	11.10	5.51	12.31	0.16	6.6×10^6
S1	1.77 ± 0.02	6.35	−2.93	−3.40	0.05	3.3×10^7
S2	1.64 ± 0.02	4.50	−9.04	−11.29	0.04	6.2×10^7
S3	1.03 ± 0.01	16.59	−8.32	−22.64	0.25	2.8×10^6

Note. Column 1: labels of the components from north to south in Fig. 1 c; Column 2: 1.5 GHz flux density and its uncertainty of the component; Column 3: full width at half-maximum of the two-dimensional Gaussian model fitted to the component; Column 4 and 5: the offset between the position of the radio component and the *Gaia* optical position in right ascension and declination, respectively; Column 6: uncertainty of the offset; Column 5: the radio brightness temperature calculated using equation (1).

being radiated out, significantly reducing the radiation efficiency. It means that the actual mass accretion rate will be even higher than predicted from the luminosity assuming typical radiation efficiencies in a standard optically thick, geometrically thin disc (Wang et al. 2014). Thus, the SMBH in Mrk 335 should reliably be a highly accreting black hole.

4.2 Origin of radio emission

Mrk 335's radio emission is relatively weak. At 1.4 GHz, de Bruyn & Wilson (1976) have observed Mrk 335 with the Westerbork telescope but were only able to set a 3σ upper limit of $f_{1.4} < 8$ mJy. Bicay et al. (1995) have observed Mrk 335 with the *Arecibo* telescope and reported an upper limit of $f_{1.4} < 5$ mJy. The observation at 2.3 GHz performed by the Parkes–Tidbinbilla Interferometer with a sub-arcsec resolution gives a flux density of $f_{2.3} = 5$ mJy (Roy et al. 1994). The observation at 20 GHz with the Owens Valley Radio Observatory reveals an upper limit of $f_{20} < 1.7$ mJy (Edelson 1987).

During the past decades, Mrk 335 has also been observed by the VLA with various angular resolutions (Table 1). The angular resolution of these observations vary from 0.″3 to 1.′5, corresponding to a linear size from 150 pc to 46 kpc. Only a compact unresolved source was found in Mrk 335 in all of these observations, and no extended emission has been detected. At 1.4 and 5 GHz, Mrk 335 shows slight variability. At 8.4 GHz, Barvainis et al. (2005) have carried out several epochs of the VLA observations between 1997 January and 1999 April, but did not find significant variability. Thus, the radio emission of Mrk 335 is compact and rather stable, with slight variability at lower frequencies. We estimate the radio spectral index between 1.4 and 8.4 GHz using the simultaneous flux measurements on 1992 February (Table 1) and obtain $\alpha_r \approx -0.6$. The spectral index between 5 and 8.4 GHz is estimate as $\alpha_r \approx -0.8$ to -1.0 using the flux measured at the angular size of 0.″3 (Table 1). If we consider the peak flux densities measured by the VLBA observations in the *L* band (1.5 GHz) and *S* band (2.3 GHz) (Section 2.1), an even steeper spectral index of $\alpha_r \sim -2$ is obtained, although the uncertainty of this index would be large due to the possible flux variability at different epochs and the low signal-to-noise ratio of the *S*-band image. While the GHz emission from the star-forming regions is usually characterized by steep spectra (Condon 1992), the steep spectral radio emission was also observed from nuclear outflows and jets (e.g. Gallimore et al. 2004; Bontempi et al. 2012). We address the contributions to the observed radio emission in Mrk 335 from star-forming activity, outflows, and jets as follows.

4.2.1 *Star-forming activity*

It was suggested that the NLS1 galaxies typically have stronger star-forming activities compared to the normal Seyfert galaxies (e.g. Deo, Crenshaw & Kraemer 2006; Sani et al. 2010). In this case, the star formation process in their dusty spirals or circumnuclear regions can have significant contributions to the radio emission. By analysing the mid-infrared (mid-IR) colours and the ratio of the radio to mid-IR flux for a sample of radio-loud NLS1 galaxies, Caccianiga et al. (2015) found that the star-forming activities can contribute a significant fraction of radio emission even in some radio-loud NLS1 galaxies. But this is not likely the case in Mrk 335. The overall radio morphology of the star-forming regions are typically extended, diffuse, and clumpy (e.g. Hummel, van der Hulst & Keel 1987; Olsson et al. 2010), while the radio images of Mrk 335 only reveal a compact source at various resolutions (e.g. Figs 1a and b). The flux densities measured at scales from tens of kpc to a few tens of parsec are quite consistent, indicating that the star-forming activity makes very little contribution to the total radio emission. This is supported by the fact that Mrk 335 has a very low star formation rate (SFR) among NLS1 galaxies. Xie et al. (2021) have estimated an SFR of $\sim 1\,M_\odot\,yr^{-1}$ based on the infrared SED and spectroscopy, which would yield a radio flux density <1 mJy at 1.5 GHz following the empirical relation derived by Condon (1992).

4.2.2 *Wind-driven outflows*

The accretion disc winds can drive wide-angle outflows, which are suggested to be prevalent in luminous AGN and are likely stronger in objects with higher Eddington ratios (e.g. Laor & Brandt 2002; Ganguly et al. 2007; Zhang et al. 2014). In the nuclear region,

these outflows have been typically observed as the blueshifted absorption lines in the UV/X-ray spectroscopy (e.g. Longinotti et al. 2019). On the galactic scales, they have been detected as the blue-wing components in the narrow emission line profiles (e.g. Komossa et al. 2008) or the molecular line profiles (e.g. Feruglio et al. 2015). The wind-driven outflows may also produce radio emission via bremsstrahlung free–free process from ionized plasma (Blundell & Kuncic 2007) or synchrotron process of the relativistic electrons accelerated by the wind shocks (Zakamska & Greene 2014), with the later being used to explain the correlation between radio emission and the [O III] line velocity width in the radio-quiet AGN (e.g. Zakamska & Greene 2014; Hwang et al. 2018). In the case of Mrk 335, evidence for outflows with velocity of a few thousand $\mathrm{km\,s^{-1}}$ is observed as blueshifted absorption lines in its X-ray and UV spectra (e.g. Longinotti et al. 2013, 2019). But, again we note that the radio images of Mrk 335 do not reveal any extended diffused radio emission on scales from kpc all the way down to a few tens of parsec. Thus, if the wind-driven uncollimated outflows have made any detectable contribution to the radio emission, it would likely originate from the central parsec-scale region.

4.2.3 Parsec-scale bipolar jet structure

On parsec scales, the VLBA image at 1.5 GHz shows a linear elongation in the north–south direction. The two-dimensional model fitting to the visibility data has revealed components in the elongated structure with the brightness temperature of $T_{\mathrm{B}} > 10^7$ K (Table 2), indicating a non-thermal, synchrotron origin. It strongly suggests that the radio emission detected on parsec scale is from the jet (Panessa et al. 2019). The offset between *Gaia* optical position and the nearest radio peak position is $\Delta \approx 5$ mas, corresponding to a projected linear offset of 2.5 pc. Taking the uncertainties in both RA and Dec. from the *Gaia* measurement (<0.1 mas) and the VLBA measurement (Table 2) into account, this offset is still significant. The nuclear optical emission is usually from the accretion disc of the central engine. If the position of the central engine is really offset from either of the radio peaks, and is located between 'N' and 'S' components, considering the symmetric jet distribution with regards to the central engine represented by *Gaia* (Fig. 1), the radio structure is likely to indicate the bipolar ejection with a moderate angle between its axis and the line of sight. The larger flux density of the south branch than the north one could be due to the beaming effect as the south jet is approaching the observers. And if the 'S' components and 'N' components represent where the jet and counterjet is located, respectively, we would derive a low jet-to-counterjet ratio of ∼2.2. A low jet-to-counterjet ratio usually results from either that the jet has a large viewing angle between its axis and the line of sight, e.g. close to the sky plane, or that the jet has a low velocity. Given that Mrk 335 is a type 1 AGN, the viewing angle is unlikely to be very large. So the low jet-to-counterjet ratio may imply a low jet speed in Mrk 335. For instance, assuming a viewing angle of 45° and a spectral index of −0.5, we obtain a jet speed of $\beta_{\mathrm{j}} = (v_{\mathrm{j}}/c) \approx 0.2$ by using the equation in Bempong-Manful et al. (2020).

The total flux density of the detected components in the VLBA image is 6.46 ± 0.06 mJy, which is similar to the measurements on larger scales taken by the VLA with poorer resolution (Table 1). Especially, the total radio flux density detected in the VLBA *L* band is consistent with the 1.4 GHz VLA flux density of 6.19 ± 0.29 mJy measured with a resolution of ∼2 arcsec (Yang et al. 2020) within uncertainty, indicating that the radio emission within 2 arcsec (corresponding to ∼1 kpc) is dominated by the central parsec-scale bipolar jet structure and that the contribution from the star-forming activity and wind-driven outflows is very small even if it cannot be totally ruled out.

We notice that the two-dimensional Gaussian models fitted to the VLBA visibility data at 1.5 GHz reveal an S-shaped distribution, likely implying a helical jet or slowly drifting of the position angle of the jet axis. One of the scenarios adopted to explain the change of the jet axis is the binary black hole system, in which the secondary black hole causes the precession of the black hole orbit or the primary accretion disc, resulting in an S-shaped jet (e.g. Roos, Kaastra & Hummel 1993; Rubinur et al. 2017). But there is not yet evidence, e.g. double-peaked emission lines, systematic line shifts, periodic behaviour, or dual bright compact radio cores, for the existence of binary black hole system in Mrk 335. Another possible mechanism causing the S-shaped jet would be the warped disc near the jet launching site, arising from non-axisymmetric radiation (Pringle 1996) or accretion events, the latter of which would be interesting given that Mrk 335 is accreting at such high Eddington ratio and has been detected for several flares in optical and X-rays during the past decades (Komossa et al. 2020). However, the current data set is not adequate to confirm the validity of they S-shaped jet structure in Mrk 335. Further observations are required to investigate the outer structures at both jet sides with medium-resolution and the inner jet structures with high-resolution, which are crucial to confirm the S-shaped jet structure and its origin.

4.3 Implications on jet formation

The jets have been widely observed in different types of accreting sources. During the past decades, great efforts have been made on theoretical work to explain the jet formation. So far, several popular models have been proposed such as the Blandford–Znajek process, in which the jet is driven by extracting the rotational energy of the black hole via a large-scale magnetic field (Blandford & Znajek 1977), and Blandford–Payne process, in which the jet is driven by extracting the rotational energy of the accretion disc via the magnetic fields threading the disc (Blandford & Payne 1982). Recently, some numerical simulations have been done for the jet formation in super-Eddington accreting SMBHs, in which the jet is driven by radiation pressure (e.g. Ohsuga & Mineshige 2011; Tchekhovskoy et al. 2014; Sądowski & Narayan 2015). However, although a lot of important progress has been made, we still do not fully understand the physical mechanism for launching the jet.

4.3.1 Analogue to galactic black holes?

The radio structure observed in Mrk 335 by VLBA provides a good evidence of jet launched by a highly accreting SMBH in the radio-quiet Seyfert galaxy. Although the detailed mechanism of jet formation is still unknown, a possible way to explore the jet formation in Mrk 335, in the framework of current knowledge, is through the comparison with other highly accreting sources. As the down-scaled analogues to the accreting SMBHs in AGN, the Galactic black holes (GBH) of stellar mass in the X-ray binaries also display the phenomenon of accretion (in X-rays) and jet (in radio). In the GBH, the steady jet is always associated with low-luminosity hard X-ray spectral state (low/hard state), while the radio emission is suppressed in the high-luminosity soft X-ray spectral state (high/soft state). In addition, an intermediate state (i.e. very high state) is also observed when GBH's soft X-ray luminosity rises to a peak and the jet becomes choked and episodic, associated with the radio outburst (Fender, Belloni & Gallo 2004).

Considering the high Eddington ratio, Mrk 335 may be the scaled-up version of GBHs at the end of their very high state. If this is the case, the radio observations may capture the evidence of its past ejecting activities during the state transition. Previous observations have found several NLS1 galaxies showing kiloparsec-scale radio structures, implying the past ejecting activities (e.g. Gliozzi et al. 2010; Doi et al. 2012; Richards & Lister 2015; Yang et al. 2020). However, such evidence has not yet been detected in Mrk 335 by observations spanning the past decades. Alternatively, Mrk 335 may have already transitioned to the high/soft state so long ago that the energy of the ejecta, if it had existed, has already dissipated, therefore kiloparsec-scale radio emission tracing the past ejecting activities is not detected. If this is the case, the elongated structure detected by our VLBA image should be newly ejected after the steady/episodic jet being switched off, which implies that the collimation of the outflows in Mrk 335 could be maintained/established on small scales even after the accreting source has transitioned to the high/soft state.

4.3.2 Comparison to tidal disruption event

Another kind of highly accreting source is the tidal disruption event (TDE; Komossa 2015), in which a star passing by an SMBH is tidally disrupted and accreted by the SMBH, leading to a bright flare with an accretion rate near or exceeding the Eddington limit. Several dozens of TDEs have been discovered based on their large-amplitude brightening in X-rays, UV, and/or optical. But so far only three TDEs have been reported to launch jets (Bloom et al. 2011; Burrows et al. 2011; Levan et al. 2011; Zauderer et al. 2011; Cenko et al. 2012; Alexander et al. 2016; van Velzen et al. 2016). For instance, as the most representative jetted–TDE, Swift J1644 + 57, which hosts an inactive galactic nuclei, has revealed an apparent luminosity $\sim 10^3$ times of the Eddington limit for its black hole mass, and an SED characterized by synchrotron and inverse Compton processes (Bloom et al. 2011; Burrows et al. 2011; Levan et al. 2011; Zauderer et al. 2011), leading inevitably to a scenario of a jet pointing to the observer. A variable radio synchrotron emission was detected a few days after the rapid rise in its X-rays (Zauderer et al. 2011), providing evidence for jet launched by the highly accreting SMBH. Recent numerical simulations of the super-Eddington compact disc used to explain the TDEs have shown that, together with a geometrically thick disc and a fast outflow, a relativistic jet can also be produced under optimal conditions given a spinning black hole and a large-scale-ordered magnetic field (Dai et al. 2018). If the accretion process in the highly accreting AGN is the same as that in the TDE, this gives hints to the jet feature in Mrk 335: the jet may be driven by the magnetic field threading the spinning SMBH and the disc, and is powered by the black hole spin energy. This is consistent with a high spin parameter measured for Mrk 335 based on the blurred reflection model fitted to the X-ray spectrum (Gallo et al. 2015, 2019). The size of the jet in Mrk 335 is very small and only resolved at parsec scales (Fig. 1). Coincidently, the radio structure in jetted-TDE was also found to be very compact (Romero-Cañizales et al. 2016; Yang et al. 2016). Considering the low jet speed and the high Eddington ratio in Mrk 335, the small size of the jet may be due to the jet deceleration by interaction with surrounding dense medium in the nuclear region.

4.3.3 Missing radio core?

In a jet structure, a parsec-scale compact radio core with flat or inverted spectrum is usually present at the position of jet base in the vicinity of accreting SMBH. As shown in Fig. 1, even taking into account the uncertainties, the optical position of Mrk 335 measured by *Gaia* does not coincide with the position of any radio components. If the optical position represents the position of the central SMBH and its accretion disc, our results imply an offset between the radio components and the central engine in Mrk 335, and we do not explicitly find the radio core near the position of the central engine.

The symmetric jet structure lacking a detectable core was also reported in other kind of radio sources such as some compact symmetric objects, in which the core is so weak due to the jet axis very close to the sky plane (e.g. Taylor et al. 2000). But this is unlikely the case in Mrk 335 as it is a type 1 AGN. We note that the emission centre in optical and radio may not always coincide due to that the centroid of the radio component may be shifted with observing frequency (Kovalev et al. 2008; Petrov & Kovalev 2017). So a possible reason for the 'missing core' in our observation may be that the core is too weak to be detected at 1.5 GHz due to the synchrotron-self-absorption at lower frequencies (Kovalev, Petrov & Plavin 2017), and it is buried in other radio components and not resolved by our observation. If this is the case, the core may reveal itself at higher frequencies. Unfortunately, the archival VLBA observation of Mrk 335 at 8.4 GHz (project ID: BB0056 and BG0093) does not reveal any detection, and only gives an upper limit of < 0.8 mJy (Blundell & Beasley 1998). Deeper VLBI observations at higher frequencies, e.g. 8.4 and 15 GHz, are needed to test if there exists a compact core.

4.3.4 Jet–corona connection

A collimated corona has been suggested to launch from the accretion disc based on the past X-ray spectroscopic observations on Mrk 335 during its X-ray flares (e.g. Wilkins & Gallo 2015; Gallo et al. 2019). Generally, the X-ray emission is produced by the hot electrons in corona above the accretion disc via inverse Compton scattering of the soft photons from disc. Then, a fraction of X-ray emission illuminates the disc and is reflected, contributing to the reflection component in the observed X-ray spectrum. During the X-ray flares of Mrk 335, it was found that the reflection fraction dropped significantly and the emissivity profile of the outer disc steepened, indicating that the corona is illuminating less to the disc, which is expected if the corona is moving away from the disc at high speed and beaming its radiation (Gallo et al. 2019). In addition, it was suggested that the AGN corona might be magnetically heated, and the radio and X-ray emission originating from the coronal activities would reveal a ratio of $\sim 10^{-5}$, similar to those in the coronally active stars (Laor & Behar 2008). Using the X-ray fluxes provided in Grupe et al. (2008) and the radio measurements in Table 1 as well as by our VLBA measurement, the flux ratio of radio-to-X-ray is in the range $\sim 10^{-6}$ to $\sim 10^{-5}$ that is similar to the suggested relation in Laor & Behar (2008). It implies the possibility that the corona is the jet base, which was also suggested by previous works, e.g. in Wilkins & Gallo (2015) and Gallo et al. (2019).

However, the ejecta in the collimated corona detected by the X-ray can only reach a height of no more than ten gravitational radius R_g as estimated in Gallo et al. (2019; see their fig. 10), while the projected scale of the jet structure detected in our VLBA image is $\sim$20 pc, corresponding to $\sim 10^7\ R_g$. It is not clear whether the parsec-scale radio jet in Mrk 335 has any relation to the collimated X-ray corona, and, if they are related, how the particles can be accelerated to such large distance from within a few R_g above the accretion disc. This may be tested by the future higher resolution radio observations

and by the correlation of simultaneous X-ray and radio monitoring observations.

5 SUMMARY

We report the VLBA observation at 1.5 GHz on a nearby radio-quiet NLS1 galaxy Mrk 335 in which its central SMBH accretes near/above Eddington limit. The image reveals an elongated jet structure extending ~ 20 parsec, with the brightness temperature as high as $\sim 6 \times 10^7$ K. This work increases the number of known parsec-scale jet in the highly accreting radio-quiet NLS1 galaxies, which is rare so far. The consistence of the flux measured by VLBA with the historical measurements at larger scales by VLA shows that the radio emission of Mrk 335 is dominated by the central parsec-scale jet. We discuss the comparison with other highly accreting jetted black holes, and the possible connection between the X-ray corona and the jet. The discovery of jet features in the highly accreting AGN will provide us with further constraints on the physics of the accretion-jet coupling in high Eddington ratio regime. In our future work, we will report results of the observations on the parse-scale nuclear region in other highly accreting radio-quiet NLS1 galaxies (Yang et al. in preparation).

ACKNOWLEDGEMENTS

SY acknowledges the support by an Alexander von Humboldt Foundation Fellowship. XLY thanks the support by Shanghai Sailing Program (21YF1455300) organized by the Science and Technology Commission of Shanghai Municipality (STCSM) and China Postdoctoral Science Foundation (2021M693267). XLY and TA thank the financial support by the National Key Research and Development Program of China (2018YFA0404603) and the Chinese Academy of Sciences (114231KYSB20170003). MFG is supported by the National Science Foundation of China (11873073). LCH, RW, and XW was supported by the National Science Foundation of China (11721303, 11991052) and the National Key Research and Development Program of China (2016YFA0400702 and 2016YFA0400703). The National Radio Astronomy Observatory (NRAO) is a facility of the National Science Foundation operated under cooperative agreement by Associated Universities, Inc. This work used the Swinburne University of Technology software correlator, developed as part of the Australian Major National Research Facilities Programme and operated under licence. This work has also used the NASA Astrophysics Data System Abstract Service (ADS), and the NASA/IPAC Extragalactic Database (NED) which is operated by the Jet Propulsion Laboratory, California Institute of Technology, under contract with the National Aeronautics and Space Administration.

DATA AVAILABILITY

The VLBA data of BY0145 will be shared on reasonable request to the corresponding author. The archival VLBA data (BB0056, BG0093) and the VLA data (AM0384) underlying this article are available in the NRAO data archive (https://science.nrao.edu/facilities/vla/archive/index). The webpage of the STCSM is: http://stcsm.sh.gov.cn/yww/

REFERENCES

Abramowicz M. A., Czerny B., Lasota J. P., Szuszkiewicz E., 1988, ApJ, 332, 646
Alexander K. D., Berger E., Guillochon J., Zauderer B. A., Williams P. K. G., 2016, ApJ, 819, L25
Barth A. J., Ho L. C., Sargent W. L. W., 2003, ApJ, 583, 134
Barvainis R., Lehár J., Birkinshaw M., Falcke H., Blundell K. M., 2005, ApJ, 618, 108
Bempong-Manful E., Hardcastle M. J., Birkinshaw M., Laing R. A., Leahy J. P., Worrall D. M., 2020, MNRAS, 496, 676
Bentz M. C., Peterson B. M., Netzer H., Pogge R. W., Vestergaard M., 2009, ApJ, 697, 160
Berton M. et al., 2018, A&A, 614, A87
Bicay M. D., Kojoian G., Seal J., Dickinson D. F., Malkan M. A., 1995, ApJS, 98, 369
Blandford R. D., Payne D. G., 1982, MNRAS, 199, 883
Blandford R. D., Znajek R. L., 1977, MNRAS, 179, 433
Bloom J. S. et al., 2011, Science, 333, 203
Blundell K. M., Beasley A. J., 1998, MNRAS, 299, 165
Blundell K. M., Kuncic Z., 2007, ApJ, 668, L103
Bontempi P., Giroletti M., Panessa F., Orienti M., Doi A., 2012, MNRAS, 426, 588
Burrows D. N. et al., 2011, Nature, 476, 421
Caccianiga A. et al., 2015, MNRAS, 451, 1795
Cenko S. B. et al., 2012, ApJ, 753, 77
Condon J. J., 1992, ARA&A, 30, 575
Condon J. J., Cotton W. D., Greisen E. W., Yin Q. F., Perley R. A., Taylor G. B., Broderick J. J., 1998, AJ, 115, 1693
Dai L., McKinney J. C., Roth N., Ramirez-Ruiz E., Miller M. C., 2018, ApJ, 859, L20
Deller A. T., Tingay S. J., Bailes M., West C., 2007, PASP, 119, 318
Deller A. T. et al., 2011, PASP, 123, 275
Deo R. P., Crenshaw D. M., Kraemer S. B., 2006, AJ, 132, 321
Doi A., Asada K., Nagai H., 2011, ApJ, 738, 126
Doi A., Nagira H., Kawakatu N., Kino M., Nagai H., Asada K., 2012, ApJ, 760, 41
Doi A., Asada K., Fujisawa K., Nagai H., Hagiwara Y., Wajima K., Inoue M., 2013, ApJ, 765, 69
Doi A., Wajima K., Hagiwara Y., Inoue M., 2015, ApJ, 798, L30
Du P. et al., 2014, ApJ, 782, 45
Edelson R. A., 1987, ApJ, 313, 651
de Bruyn A. G., Wilson A. S., 1976, A&A, 53, 93
Elvis M. et al., 1994, ApJS, 95, 1
Fabian A. C., 2012, ARA&A, 50, 455
Falomo R., Kotilainen J. K., Treves A., 2002, ApJ, 569, L35
Fender R. P., Belloni T. M., Gallo E., 2004, MNRAS, 355, 1105
Feruglio C. et al., 2015, A&A, 583, A99
Gaia Collaboration, 2016, A&A, 595, A1
Gallimore J. F., Baum S. A., O'Dea C. P., 2004, ApJ, 613, 794
Gallo L. C. et al., 2015, MNRAS, 446, 633
Gallo L. C., Blue D. M., Grupe D., Komossa S., Wilkins D. R., 2018, MNRAS, 478, 2557
Gallo L. C. et al., 2019, MNRAS, 484, 4287
Ganguly R., Brotherton M. S., Cales S., Scoggins B., Shang Z., Vestergaard M., 2007, ApJ, 665, 990
Giroletti M., Panessa F., 2009, ApJ, 706, L260
Gliozzi M., Papadakis I. E., Grupe D., Brinkmann W. P., Raeth C., Kedziora-Chudczer L., 2010, ApJ, 717, 1243
Greene J. E., Ho L. C., Ulvestad J. S., 2006, ApJ, 636, 56
Greisen E. W., 2003, in Heck A., ed., AIPS, Information Handling in Astronomy - Historical Vistas, Astrophysics and Space Science Library Vol. 285,. Springer, Dordrecht. p. 109
Grier C. J. et al., 2012, ApJ, 744, L4
Grupe D., Komossa S., Gallo L. C., Fabian A. C., Larsson J., Pradhan A. K., Xu D., Miniutti G., 2008, ApJ, 681, 982
Gu M., Chen Y., Komossa S., Yuan W., Shen Z., Wajima K., Zhou H., Zensus J. A., 2015, ApJS, 221, 3
Ho L. C., 2002, ApJ, 564, 120
Ho L. C., 2008, ARA&A, 46, 475
Hovatta T., Lister M. L., Aller M. F., Aller H. D., Homan D. C., Kovalev Y. Y., Pushkarev A. B., Savolainen T., 2012, AJ, 144, 105

Huchra J. P., Vogeley M. S., Geller M. J., 1999, ApJS, 121, 287
Hummel E., van der Hulst J. M., Keel W. C., 1987, A&A, 172, 32
Hwang H.-C., Zakamska N. L., Alexandroff R. M., Hamann F., Greene J. E., Perrotta S., Richards G. T., 2018, MNRAS, 477, 830
Ivezić Ž. et al., 2002, AJ, 124, 2364
Kellermann K. I., Sramek R., Schmidt M., Shaffer D. B., Green R., 1989, AJ, 98, 1195
Kim M., Ho L. C., Peng C. Y., Barth A. J., Im M., 2017, ApJS, 232, 21
Komossa S., 2015, J. High Energy Astrophys., 7, 148
Komossa S., Xu D., Zhou H., Storchi-Bergmann T., Binette L., 2008, ApJ, 680, 926
Komossa S. et al., 2020, A&A, 643, L7
Kormendy J., Ho L. C., 2013, ARA&A, 51, 511
Kovalev Y. Y., Lobanov A. P., Pushkarev A. B., Zensus J. A., 2008, A&A, 483, 759
Kovalev Y. Y., Petrov L., Plavin A. V., 2017, A&A, 598, L1
Kukula M. J., Pedlar A., Baum S. A., O'Dea C. P., 1995, MNRAS, 276, 1262
Lal D. V., Shastri P., Gabuzda D. C., 2004, A&A, 425, 99
Laor A., Behar E., 2008, MNRAS, 390, 847
Laor A., Brandt W. N., 2002, ApJ, 569, 641
Leipski C., Falcke H., Bennert N., Hüttemeister S., 2006, A&A, 455, 161
Levan A. J. et al., 2011, Science, 333, 199
Longinotti A. L. et al., 2013, ApJ, 766, 104
Longinotti A. L. et al., 2019, ApJ, 875, 150
McMullin J. P., Waters B., Schiebel D., Young W., Golap K., 2007, in Shaw R. A., Hill F., Bell D. J., eds, ASP Conf. Ser. Vol. 376, Astronomical Data Analysis Software and Systems XVI. Astron.Soc. Pac.,San Fransisco, p.127
Middelberg E. et al., 2004, A&A, 417, 925
Miller P., Rawlings S., Saunders R., 1993, MNRAS, 263, 425
Mineshige S., Kawaguchi T., Takeuchi M., Hayashida K., 2000, PASJ, 52, 499
Mundell C. G., Wrobel J. M., Pedlar A., Gallimore J. F., 2003, ApJ, 583, 192
Nagar N. M., Wilson A. S., Mulchaey J. S., Gallimore J. F., 1999, ApJS, 120, 209
Ohsuga K., Mineshige S., 2011, ApJ, 736, 2
Olsson E., Aalto S., Thomasson M., Beswick R., 2010, A&A, 513, A11
Pan X. et al., 2021, ApJ, 912, 118
Panessa F., Giroletti M., 2013, MNRAS, 432, 1138
Panessa F., Baldi R. D., Laor A., Padovani P., Behar E., McHardy I., 2019, Nat. Astron., 3, 387
Peterson B. M. et al., 2004, ApJ, 613, 682
Petrov L., Kovalev Y. Y., 2017, MNRAS, 467, L71
Pringle J. E., 1996, MNRAS, 281, 357
Richards J. L., Lister M. L., 2015, ApJ, 800, L8
Romero-Cañizales C., Prieto J. L., Chen X., Kochanek C. S., Dong S., Holoien T. W. S., Stanek K. Z., Liu F., 2016, ApJ, 832, L10
Roos N., Kaastra J. S., Hummel C. A., 1993, ApJ, 409, 130
Roy A. L., Norris R. P., Kesteven M. J., Troup E. R., Reynolds J. E., 1994, ApJ, 432, 496
Rubinur K., Das M., Kharb P., Honey M., 2017, MNRAS, 465, 4772
Sani E., Lutz D., Risaliti G., Netzer H., Gallo L. C., Trakhtenbrot B., Sturm E., Boller T., 2010, MNRAS, 403, 1246
Shepherd M. C., 1997, in Hunt G., Payne H., eds, ASP Conf. Ser. Vol. 125, Astronomical Data Analysis Software and Systems VI.Astron. Soc. Pac.,San Fransisco, p.77
Sikora M., Stawarz Ł., Lasota J.-P., 2007, ApJ, 658, 815
Sądowski A., Narayan R., 2015, MNRAS, 453, 3213
Taylor G. B., Marr J. M., Pearson T. J., Readhead A. C. S., 2000, ApJ, 541, 112
Tchekhovskoy A., Metzger B. D., Giannios D., Kelley L. Z., 2014, MNRAS, 437, 2744
Tripathi S., McGrath K. M., Gallo L. C., Grupe D., Komossa S., Berton M., Kriss G., Longinotti A. L., 2020, MNRAS, 499, 1266
Ulvestad J. S., Antonucci R. R. J., Barvainis R., 2005, ApJ, 621, 123
Urry C. M., Padovani P., 1995, PASP, 107, 803
van Velzen S. et al., 2016, Science, 351, 62
Vasudevan R. V., Fabian A. C., 2009, MNRAS, 392, 1124
Wang A., An T., Jaiswal S., Mohan P., Wang Y., Baan W. A., Zhang Y., Yang X., 2021, MNRAS, 504, 3823
Wang J.-M., Du P., Valls-Gabaud D., Hu C., Netzer H., 2013, Phys. Rev. Lett., 110, 081301
Wang J.-M. et al., 2014, ApJ, 793, 108
Wilkins D. R., Gallo L. C., 2015, MNRAS, 449, 129
Xie Y., Ho L. C., Zhuang M.-Y., Shangguan J., 2021, ApJ, 910, 124
Yang J., Paragi Z., van der Horst A. J., Gurvits L. I., Campbell R. M., Giannios D., An T., Komossa S., 2016, MNRAS, 462, L66
Yang X. et al., 2020, ApJ, 904, 200
Yuan W., Zhou H. Y., Komossa S., Dong X. B., Wang T. G., Lu H. L., Bai J. M., 2008, ApJ, 685, 801
Zakamska N. L., Greene J. E., 2014, MNRAS, 442, 784
Zauderer B. A. et al., 2011, Nature, 476, 425
Zhang S., Wang H., Wang T., Xing F., Zhang K., Zhou H., Jiang P., 2014, ApJ, 786, 42
Zhou H., Wang T., Yuan W., Lu H., Dong X., Wang J., Lu Y., 2006, ApJS, 166, 128

This paper has been typeset from a TEX/LATEX file prepared by the author.